

Disturbance Compensation for Safe Kinematic Control of Robotic Systems with Closed Architecture

Fan Zhang^{1,2*}, Jinfeng Chen^{1*}, Joseph J. B. Mvogo Ahanda³, Hanz Richter⁴, Ge Lv⁵, Bin Hu^{1,2}, Qin Lin^{1,2}

Abstract—In commercial robotic systems, it is common to encounter a closed inner-loop torque controller that is not user-modifiable. However, the outer-loop controller, which sends kinematic commands such as position or velocity for the inner-loop controller to track, is typically exposed to users. In this work, we focus on the development of an easily integrated add-on at the outer-loop layer by combining disturbance rejection control and robust control barrier function for high-performance tracking and safe control of the whole dynamic system of an industrial manipulator. This is particularly beneficial when 1) the inner-loop controller is imperfect, unmodifiable, and uncertain; and 2) the dynamic model exhibits significant uncertainty. Stability analysis, formal safety guarantee proof, and hardware experiments with a PUMA robotic manipulator are presented. Our solution demonstrates superior performance in terms of simplicity of implementation, robustness, tracking precision, and safety compared to the state of the art. Video: <https://youtu.be/zw1tanvrV8Q>

Index Terms—Disturbance Compensation, Robust Control Barrier Function, Extended State Observer, High-Performance Tracking, Safe Control.

I. INTRODUCTION

Robotic systems typically use a hierarchical architecture combining perception, planning, and low-level control, which improves modularity and reliability. In the control layer, a *kinematic controller* (outer loop) and a *dynamic controller* (inner loop) are commonly used. Since tuning the inner loop requires expertise, it is usually hidden from users for safety, forming a *closed architecture* [1]–[4]. Users can thus only design the kinematic controller, sending position or velocity commands. However, wear, modifications, or payload changes can alter dynamics and degrade inner-loop performance [5]. This work addresses the challenge of achieving unified high-performance and safe tracking control using only the kinematic controller, despite an imperfect, unmodifiable inner loop, and uncertain dynamics.

Fig. 1 shows that our approach successfully follows an infinity-shaped reference trajectory despite various uncertain-



Fig. 1. Trajectory tracking of the PUMA 500 for an infinity-shaped reference.

ties and a poor inner-loop unknown controller (see the blue trajectory). In contrast, using the poor inner-loop controller without our approach’s compensation results in poor trajectory tracking (see the red trajectory).

A detailed literature review can be found in the subsequent section. Existing works typically rely on the following assumptions: 1) The inner-loop controller is known and accessible to the user; 2) The inner-loop controller is known but not accessible to the user; 3) The inner-loop controller has perfect tracking for outer-loop commands. Our goal is to minimize reliance on knowledge of the dynamic model and the inner-loop controller, while still guaranteeing tracking and safe control using only an outer-loop kinematic controller.

As shown in Fig. 2, existing robotic systems typically send desired position (q^*) or velocity (\dot{q}^*) commands to the inner-loop controller. Our solution, inserted between them (gray box), comprises a disturbance-rejection tracking controller, an extended state observer (ESO), and an extended state observer-based robust quadratic programming (ESOR-QP) module. The ESO estimates the total disturbance \hat{f} using the joint angle q and the safe kinematic control $q_{d,\text{safe}}$ or $\dot{q}_{d,\text{safe}}$. This estimate is compensated in the tracking controller to produce nominal commands q_d or \dot{q}_d , which are monitored by the ESOR-QP to enforce robust safety constraints.

The contributions of our work are summarized as follows:

- We innovatively formulate the kinematic control of closed-architecture robotic manipulator systems as a dis-

¹The authors are with the Department of Engineering Technology, University of Houston, USA. Corresponding author: Qin Lin.

²These authors are also with the Department of Electrical and Computer Engineering, University of Houston, USA

³Joseph Jean Baptiste Mvogo Ahanda is with the Department of Biomedical Engineering, The University of Ebolowa, Cameroon.

⁴Hanz Richter is with the Department of Mechanical Engineering, Cleveland State University, USA.

⁵Ge Lv is with the Department of Mechanical Engineering, Clemson University, USA.

*These authors contribute equally.

turbance rejection problem, requiring only a practical assumption on the structure, Jacobian, and nominal inertia matrix.

- We develop a robust control barrier function (CBF) framework based on an extended state observer, enabling safe control of general nonlinear affine systems with high relative degrees under disturbances. To the best of our knowledge, this is the first work achieving safe kinematic control of closed-architecture robots under largely unknown uncertainties.
- As shown in Fig. 2, our method is implemented as a standalone add-on module that enhances existing robotic manipulators without modifying the inner-loop controller. Real-time control at 1 kHz is demonstrated on a PUMA 500 manipulator.

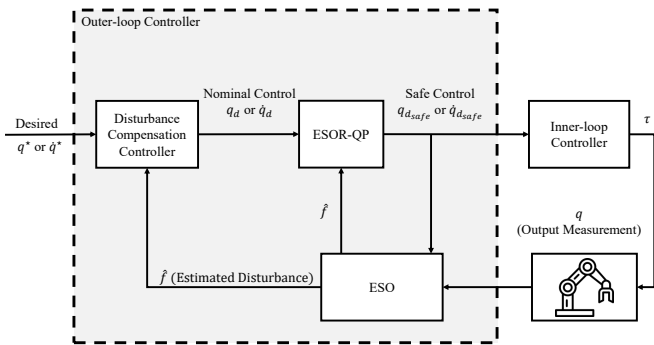


Fig. 2. The proposed framework in this paper, is marked as the Outer-loop Controller. The total estimated disturbance \hat{f} is used for both disturbance compensation and safe control using ESOR-QP.

The rest of the paper is organized as follows: Section II reviews the related work. Section III introduces the preliminaries and problem formulation. Section IV presents the proposed framework. Hardware experiments are reported in Section V. Concluding remarks are in Section VI.

II. RELATED WORK

An overview of the comparison between our work and the most related works is presented in Table I.

A. Adaptive Control for Closed Architecture

Learning-based Adaptive Control: [2]–[4] employ neural network-based outer-loop adaptation to approximate the kinematics, dynamics, and inner-loop controller. As summarized in Table I, they make the weakest assumption about the inner loop, identical to ours, where $\Psi(\cdot)$ denotes an unknown structure possibly containing proportional, integral, or state-dependent terms. However, they rely on numerous tuning parameters and limited interpretability.

Conventional Adaptive Control: [1] introduces dynamic modularity with an adaptive controller under a moderate assumption of a known PI/PID inner-loop structure.

These studies address tracking control only, without safety considerations. In our experiments, we compare tracking performance with the learning-based adaptive control due to the shared inner-loop assumption.

B. Reduced-order Model-based CBF

Many CBF-based safety approaches rely on high-fidelity dynamic models with torque control, yet obtaining such models remains challenging. Reduced-order or kinematic CBFs have been introduced to ensure safety with lower-fidelity models. For instance, [6] guarantees safety via safe velocity control but assumes a perfect inner-loop controller capable of instant tracking. Similarly, [7], [8] employ kinetic energy-based CBFs that offer partial robustness to model uncertainty but still depend on numerous dynamic parameters and a known PD-type inner loop. In contrast, our work addresses closed-architecture robots with minimal knowledge of the inner-loop controller and significant model uncertainty.

C. Robust CBF

Robust CBFs have recently been developed to handle model uncertainties and external disturbances [9]–[25]. Among them, disturbance observer-based robust CBFs (DOB-CBFs) [15]–[25] enable active disturbance estimation without requiring worst-case bounds. Unlike these methods where estimation error bounds are absent or loosely derived via Lyapunov analysis, our approach obtains them directly from the observer error dynamics, resulting in tighter and less conservative bounds. Experimental comparisons with state-of-the-art methods (e.g., [16]) further demonstrate this advantage. In contrast to our conference version [25] that only considered relative-degree-one systems, this work provides a generalized framework with rigorous proofs guaranteeing the forward invariance of the safety set.

III. PRELIMINARY AND PROBLEM FORMULATION

A. System Dynamics

We consider a general robotic system with an Euler–Lagrange formulation incorporating a generalized external disturbance force F_{ext} :

$$\begin{cases} M\ddot{q} + C\dot{q} + G + F_r = \tau + J^T F_{ext} \\ y = \zeta(q) \end{cases}, \quad (1)$$

where $q, \dot{q}, \ddot{q} \in \mathbb{R}^n$ are the joint position, velocity, and acceleration, respectively. $M \in \mathbb{R}^{n \times n}$ is the symmetric positive-definite inertia matrix; $C \in \mathbb{R}^{n \times n}$ denotes centrifugal and Coriolis term; $G \in \mathbb{R}^n$ is the gravity term; $F_r \in \mathbb{R}^n$ accounts for the friction torque; $\tau \in \mathbb{R}^n$ represents the torque (provided by the inner-loop controller); $J \in \mathbb{R}^{6 \times n}$ is the Jacobian matrix; and $F_{ext} \in \mathbb{R}^6$ represents a generalized external disturbance force. The output $y \in \mathbb{R}^m$, and $\zeta: \mathbb{R}^n \rightarrow \mathbb{R}^m$ is the mapping from joint space to task space.

The most common inner-loop controller for robot manipulators typically consists of a PID controller or PD controller, often combined with dynamic compensation, such as gravity. For stability, most inner-loop controllers include a derivative term for damping, $(\dot{q} - \dot{q}_d)$, where \dot{q}_d is a joint velocity command.

Assumption 1: We assume the inner-loop controller has the following structure:

$$\tau = -K_d(\dot{q} - \dot{q}_d) + \Psi(q, \dot{q}, q_d, \int_0^t \dot{q} dt, \int_0^t q_d dt), \quad (2)$$

TABLE I
OVERVIEW OF OUR WORK'S POSITION IN THE LITERATURE

Methods	Tracking	Safety	Assumption of Inner-loop Controller	Ref.
Learning-based Adaptive Control	✓	✗	Weak $\tau = -K_d(\dot{q} - \dot{q}_d) + \Psi(q, \dot{q}, q_d, \int_0^t q dt, \int_0^t q_d dt)$	[2]–[4]
Conventional Adaptive Control	✓	✗	Moderate, known PID/PI structure	[1]
Reduced-order CBF	-	✓	Strong, known PD structure, perfect tracking or bounded error	[6]–[8]
Robust CBF	-	✓	-	[9]–[24]
Ours	✓	✓	Weak $\tau = -K_d(\dot{q} - \dot{q}_d) + \Psi(q, \dot{q}, q_d, \int_0^t q dt, \int_0^t q_d dt)$	-

The two dashes for CBFs' tracking indicate that we only compare our safety performance with them, as their nominal tracking controllers vary significantly across papers. The third dash for the robust CBF indicates that those works do not consider two-loop controllers.

with K_d a proportional control gain, and $\Psi(\cdot)$ is a general, unknown function that may include proportional, integral, derivative, and dynamic compensation terms. To the best of our knowledge, this assumption is the most general in the literature (see Table I), requiring minimal knowledge of the inner-loop controller, similar to [2], and more general than [1].

Assumption 2: The kinematics of the system are assumed to be known for control in task space.

The system dynamic model combining (1) and (2) is:

$$\ddot{q} = M^{-1} \left(-C\dot{q} - G - F_r + J^T F_{ext} - K_d\dot{q} + \Psi(\cdot) + K_d\dot{q}_d \right). \quad (3)$$

We have removed torque control, as it is not accessible in a closed architecture. \dot{q}_d is the kinematic control to be manipulated in the outer-loop layer, and its control law will be designed. Another reason for choosing \dot{q}_d instead of q_d as the control input is to avoid differentiation-induced noise.

B. Robot Kinematic Control with Known Model

Neglecting F_r and F_{ext} in (1), the exact system dynamics is used to design the control law:

$$\dot{q}_d = K_d^{-1} \left(M u_0 + C\dot{q} + G + K_d\dot{q} - \Psi(\cdot) \right), \quad (4)$$

where the position control input u_0 is defined as follows:

$$u_0 = \ddot{q}^* + k_p(q^* - q) + k_d(\dot{q}^* - \dot{q}), \quad (5)$$

where $\ddot{q}^*, \dot{q}^*, q^* \in \mathbb{R}^n$ represent the desired acceleration, velocity, and position of a reference joint trajectory generated by an upstream planner. $k_p \in \mathbb{R}^{n \times n}$ and $k_d \in \mathbb{R}^{n \times n}$ are the proportional and derivative gain matrices, respectively. \ddot{q}^* serves only as a feedforward term, while u_0 is a position controller. By substituting (4) and (5) into (3), we get:

$$\ddot{q} = \ddot{q}^* + k_p(q^* - q) + k_d(\dot{q}^* - \dot{q}). \quad (6)$$

Proper k_p and k_d make q converge to q^* asymptotically.

C. Control Barrier Functions

The system (3) can be rewritten as a nonlinear control-affine system when ignoring the disturbance vector F_{ext} :

$$\dot{x} = \psi(x) + g(x)u, \quad (7)$$

where $x \triangleq [q, \dot{q}]^T \in \mathcal{X} \subset \mathbb{R}^{2n}$, $\psi: \mathbb{R}^{2n} \rightarrow \mathbb{R}^{2n}$ and $g: \mathbb{R}^{2n} \rightarrow \mathbb{R}^{2n \times n}$ are Lipschitz continuous, and $u \triangleq \dot{q}_d \in \mathcal{U} \subset \mathbb{R}^n$ is a control input vector.

The safety of system (7) can be guaranteed using a safety set. A set \mathcal{C} is considered to be a safety set if it is forward invariant in the state space \mathcal{X} , i.e., for system (7) if solutions for some $u \in \mathcal{U}$ starting at any initial safe condition $x(0) \in \mathcal{C}$ satisfy $x(t) \in \mathcal{C}$, $\forall t \geq 0$. The safety set \mathcal{C} is defined as a 0-superlevel set of a continuously-differential function $h(x): \mathbb{R}^{2n} \rightarrow \mathbb{R}$ as:

$$\mathcal{C} = \{x \in \mathbb{R}^{2n} \mid h(x) \geq 0\}. \quad (8)$$

The function h is used to synthesize a controller with safety guarantees via a CBF.

Definition 1: (Exponential CBF (ECBF) [26], [27]) Consider system (7) with relative degree r for an r -times continuously differentiable function h , i.e., $L_g L_\psi h(x) = \dots = L_g L_\psi^{r-2} h(x) = 0$ and $L_g L_\psi^{r-1} h(x) \neq 0, \forall x \in \mathcal{C}$. $h(x)$ is an ECBF if there exists a row vector $K_a \in \mathbb{R}^r$ satisfying $\forall x \in \mathcal{C}$

$$\sup_{u \in \mathcal{U}} (L_\psi^r h(x) + L_g L_\psi^{r-1} h(x)u) \geq -K_a \eta_b(x), \quad (9)$$

where $\eta_b(x) = [h(x), \dot{h}(x), \dots, h^{(r-1)}(x)]^T$, $K_a = [k_1, \dots, k_r]$, and the values of k_1, \dots, k_r satisfy specific properties given in [26], [27].

To guarantee safety, the control problem is formulated as a quadratic program (QP) with a CBF as a hard constraint [28]:

$$u^*(x) = \arg \min_{u \in \mathcal{U}} \|u - k(x)\|^2 \quad (10)$$

$$\text{s.t. } L_\psi^r h(x) + L_g L_\psi^{r-1} h(x)u \geq -K_a \eta_b(x),$$

where $k(x)$ is a nominal control law.

Research Objective: Given the system in (3), the nominal dynamics with limited knowledge of the system and inner-loop controller are defined as

$$\ddot{q} = \bar{M}^{-1}(-\bar{C}\dot{q} - \bar{G} + \bar{K}_d\dot{q}_d), \quad (11)$$

where \bar{M} , \bar{C} , and \bar{G} are nominal parameters, and \bar{K}_d is the nominal inner-loop gain. The goal is to design a \dot{q}_d controller that achieves accurate trajectory tracking and task-space safety (e.g., collision avoidance) under an unknown inner-loop controller, uncertain dynamics, and external disturbances.

Remark 1: \bar{C} and \bar{G} can be a zero matrix and a zero vector, respectively, with minimal knowledge of the system. We use \bar{C} and \bar{G} here to make the formulation more general. The model (11) can be further reduced to:

$$\ddot{q} = \bar{M}^{-1}\bar{K}_d\dot{q}_d. \quad (12)$$

We use the nominal model (11) for general mathematical derivation, whereas the reduced nominal model (12) is employed in hardware experiments to evaluate the tracking performance and safety under limited information.

IV. PROPOSED FRAMEWORK

A. Robot Kinematic Control with Nominal Model

The control law in (4) is ideal, assuming known dynamics and an inner-loop controller. To handle uncertainties, we propose the following practical law based on nominal dynamics:

$$\dot{q}_d = \bar{K}_d^{-1}(\bar{M}u_0 + \bar{C}\dot{q} + \bar{G}). \quad (13)$$

The following part shows the dynamics of the close-loop system with our nominal control law (13). We define the parametric discrepancies as:

$$\begin{aligned} \Delta K_d &\triangleq K_d \bar{K}_d^{-1}, \\ \Delta M &\triangleq \Delta K_d \bar{M} - M, \\ \Delta C &\triangleq \Delta K_d \bar{C} - C, \\ \Delta G &\triangleq \Delta K_d \bar{G} - G. \end{aligned} \quad (14)$$

By rearranging (3), we get:

$$\begin{aligned} M\ddot{q} + C\dot{q} + G + F_r \\ = -K_d(\dot{q} - \dot{q}_d) + \Psi(\cdot) + J^T F_{ext}. \end{aligned} \quad (15)$$

Substituting (13) and (14) into (15), the right-hand side of (15) becomes:

$$\begin{aligned} -K_d\dot{q} + K_d\bar{K}_d^{-1}(\bar{M}u_0 + \bar{C}\dot{q} + \bar{G}) + \Psi(\cdot) + J^T F_{ext} \\ = -K_d\dot{q} + \Delta K_d(\bar{M}u_0 + \bar{C}\dot{q} + \bar{G}) + \Psi(\cdot) + J^T F_{ext}. \end{aligned} \quad (16)$$

The left-hand side of (15) becomes:

$$\begin{aligned} (\Delta K_d \bar{M} - \Delta M)\ddot{q} + (\Delta K_d \bar{C} - \Delta C)\dot{q} \\ + (\Delta K_d \bar{G} - \Delta G) + F_r. \end{aligned} \quad (17)$$

The resulting close-loop system is:

$$\ddot{q} = \ddot{q}^* + k_p(q^* - q) + k_d(\dot{q}^* - \dot{q}) + f. \quad (18)$$

where

$$\begin{aligned} f = (\Delta K_d \bar{M})^{-1}(\Delta M\ddot{q} + \Delta C\dot{q} + \Delta G - F_r \\ + \Psi(\cdot) + J^T F_{ext} - K_d\dot{q}). \end{aligned} \quad (19)$$

Let f denote the total disturbance, including internal uncertainties and external disturbances. Compared with (6), f degrades system performance. To counter this, an ESO [29] is employed to estimate f for disturbance rejection.

B. Extended State Observer Design

For the i -th joint of the robotic manipulator (11), we have the following second-order subsystem:

$$\begin{cases} \dot{x}_{1i} = x_{2i} \\ \dot{x}_{2i} = F_i(x) + G_i(x)\dot{q}_{di} + f_i, \end{cases} \quad (20)$$

where $x_{1i} = q_i$; $x_{2i} = \dot{q}_i$; $F_i(x)$, $G_i(x)$, and f_i are the i -th row of $F = \bar{M}^{-1}(-\bar{C}\dot{q} - \bar{G}) \in \mathbb{R}^n$, $G = \bar{M}^{-1}\bar{K}_d \in \mathbb{R}^n$, and f , respectively.

By treating f_i as an extended state, the augmented system can be written as:

$$\begin{cases} \dot{x}_{1i} = x_{2i} \\ \dot{x}_{2i} = F_i(x) + G_i(x)\dot{q}_{di} + x_{3i} \\ \dot{x}_{3i} = \hat{f}_i. \end{cases} \quad (21)$$

In many robotic systems, both joint position q and velocity \dot{q} are measurable, enabling the design of second- or third-order ESOs based on (21). With velocity measurements available, a second-order ESO is proposed for the i -th joint to estimate f_i ; otherwise, it can be readily extended to a third-order form.

The second-order ESO can be designed as:

$$\begin{cases} \dot{\hat{x}}_{2i} = F_i(x) + G_i(x)\dot{q}_{di} + \hat{x}_{3i} + \beta_{1i}(x_{2i} - \hat{x}_{2i}) \\ \dot{\hat{x}}_{3i} = \beta_{2i}(x_{2i} - \hat{x}_{2i}), \end{cases} \quad (22)$$

where \hat{x}_{2i} and \hat{x}_{3i} are the estimated velocity for \dot{q}_i and estimated disturbance for f_i , respectively. β_{1i} and β_{2i} are observer gains. The estimation error dynamic is derived from (21) and (22):

$$\dot{\vartheta}_i = A_i\vartheta_i + E_i\hat{f}_i, \quad (23)$$

where $\vartheta_i = \begin{bmatrix} x_{2i} - \hat{x}_{2i} \\ x_{3i} - \hat{x}_{3i} \end{bmatrix}$, $A_i = \begin{bmatrix} -\beta_{1i} & 1 \\ -\beta_{2i} & 0 \end{bmatrix}$, $E_i = \begin{bmatrix} 0 \\ 1 \end{bmatrix}$.

The observer gains are chosen such that the eigenvalues of the matrix A_i are placed at $-\omega_{oi}$, where ω_{oi} is the only tunable value known as the observer bandwidth [30].

C. Controller Design

\hat{f} can be used to develop a disturbance rejection controller that complements the control law (13):

$$\begin{aligned} \dot{q}_d &= \dot{q}_{d_0} + \dot{q}_{d_f}, \\ \dot{q}_{d_0} &= \bar{K}_d^{-1}(\bar{M}u_0 + \bar{C}\dot{q} + \bar{G}), \\ \dot{q}_{d_f} &= -\bar{K}_d^{-1}\bar{M}\hat{f}, \end{aligned} \quad (24)$$

where \dot{q}_{d_0} is the nominal control from (13), \dot{q}_{d_f} rejects disturbance, and they are summed to get \dot{q}_d .

D. Controller Stability Analysis

Assumption 3: There exists a positive known constant l_f such that for any $x \in \mathcal{X}$, $u \in \mathcal{U}$, and $t \geq 0$, the following inequality holds:

$$\left| \frac{\partial f_i(t, x, u)}{\partial t} \right| \leq l_f. \quad (25)$$

Assumption 3 implies that f is locally Lipschitz continuous with respect to time, and \dot{f} is bounded.

Theorem 1: Given the robotic system (3) with kinematic control input, the ESO (22) with appropriate observer bandwidth ω_{o_i} for each joint, and the nominal control law (24) with appropriate tuned k_p and k_d , we have the following properties: (i): the closed-loop system of (3) is bounded stable if each ω_{o_i} is finite; (ii): the closed-loop system of (3) is asymptotically stable if each ω_{o_i} approaches infinity.

Proof 1: Since A_i is Hurwitz, we have the following decomposition [31, Chapter 1.3]:

$$e^{A_i t} = P_i e^{\Lambda_i t} P_i^{-1}, \quad (26)$$

where P_i is a matrix whose columns are the eigenvectors of A_i , and Λ_i is a diagonal matrix with the corresponding eigenvalues in the diagonal elements.

Therefore, there exists a constant c_{1_i} such that [31, Chapter 1.9]

$$\|e^{A_i t}\| \leq \|P_i\| \|e^{\Lambda_i t}\| \|P_i^{-1}\| = c_{1_i} \|e^{\Lambda_i t}\| \leq c_{1_i} \|e^{a_i t}\|, \quad (27)$$

where a_i is the $\lambda_{max}(\Lambda_i)$, the maximum eigenvalue of Λ_i , which, in our case, is $-\omega_{o_i}$.

The solution to the error dynamics in (23) is given by:

$$\vartheta_i = e^{A_i(t-t_0)} \vartheta_i(t_0) + \int_{t_0}^t e^{A_i(t-\tau)} E \dot{f}_i(\tau) d\tau, \quad (28)$$

where t_0 is the initial time. Substituting (27) into (28), we obtain:

$$\begin{aligned} \|\vartheta_i\| &\leq c_{1_i} \|e^{-\omega_{o_i}(t-t_0)}\| \|\vartheta_i(t_0)\| \\ &\quad + \int_{t_0}^t c_{1_i} \|e^{-\omega_{o_i}(t-\tau)}\| \|E \dot{f}_i(\tau)\| d\tau \\ &\leq c_{1_i} \|e^{-\omega_{o_i}(t-t_0)}\| \|\vartheta_i(t_0)\| \\ &\quad + \frac{c_{1_i}}{\omega_{o_i}} \sup_{\tau \in (t_0, t)} \|E \dot{f}_i(\tau)\|. \end{aligned} \quad (29)$$

Since \dot{f}_i is bounded, $e^{-\omega_{o_i}(t-t_0)}$ decays exponentially, the estimation error $\|\vartheta_i\| \leq \sigma_i$ is bounded. With ω_{o_i} approaching infinity, σ_i approaches 0.

Thus, the disturbance estimation error satisfies:

$$\|\tilde{f}\| = \|f - \hat{f}\| \leq \sigma. \quad (30)$$

For the i -th joint subsystem, substituting the control law (24) into (3) results in the following i -th closed-loop subsystem dynamics:

$$\ddot{q}_i = \ddot{q}_i^* + k_{p_i}(q_i^* - q_i) + k_{d_i}(\dot{q}_i^* - \dot{q}_i) + \tilde{f}_i, \quad (31)$$

where $\tilde{f}_i = f_i - \hat{f}_i$ represents the disturbance estimation error. The error dynamic can be expressed as:

$$\dot{\epsilon} = H\epsilon + \xi, \quad (32)$$

where $\epsilon = \begin{bmatrix} q_i - q_i^* \\ \dot{q}_i - \dot{q}_i^* \end{bmatrix}$, $H = \begin{bmatrix} 0 & 1 \\ -k_{p_i} & -k_{d_i} \end{bmatrix}$, and $\xi = \begin{bmatrix} 0 \\ \tilde{f}_i \end{bmatrix}$.

The matrix H can be designed to be Hurwitz. Choose $V = \frac{1}{2}\epsilon^T Q \epsilon$ as the Lyapunov function candidate. Its derivative along (32) is given by:

$$\dot{V} = \frac{1}{2}(\dot{\epsilon}^T Q \epsilon + \epsilon^T Q \dot{\epsilon}) = -\|\epsilon\|^2 + \xi^T Q \epsilon. \quad (33)$$

By applying the Cauchy–Schwarz inequality, we obtain:

$$\dot{V} \leq -\|\epsilon\|^2 + \|\xi\| \|Q\| \|\epsilon\|. \quad (34)$$

Given that Q is positive definite, $\|Q\| \leq \lambda_{max}(Q)$, and the ξ is bounded by σ , the inequality (34) becomes:

$$\dot{V} \leq -\|\epsilon\|^2 + \sigma \lambda_{max}(Q) \|\epsilon\|. \quad (35)$$

Next, using the inequality:

$$\sigma \lambda_{max}(Q) \|\epsilon\| \leq \frac{1}{2} \|\epsilon\|^2 + \frac{1}{2} \sigma^2 \lambda_{max}^2(Q), \quad (36)$$

(35) can be rewritten as:

$$\begin{aligned} \dot{V} &\leq -\frac{1}{2} \|\epsilon\|^2 + \frac{1}{2} \sigma^2 \lambda_{max}^2(Q) \\ &\leq -\frac{V}{\lambda_{max}(Q)} + \frac{1}{2} \sigma^2 \lambda_{max}^2(Q). \end{aligned} \quad (37)$$

Solving the inequality (37) yields:

$$V \leq (v(0) - \frac{\kappa}{\eta}) e^{-\eta t} + \frac{\kappa}{\eta}, \quad (38)$$

where $\eta = \frac{1}{\lambda_{max}(Q)}$ and $\kappa = \frac{1}{2} \sigma^2 \lambda_{max}^2(Q)$. 1) It can be concluded from (38) that the states of the closed-loop system are bounded. 2) Moreover, as ω_o approaches infinity, σ approaches zero, reducing the disturbance estimation error. Consequently, the inequality (35) is simplified as $\dot{V} \leq -\eta V$, which implies that the system is asymptotically stable.

E. Robust CBF for Safe Control

By adding the disturbance term, system (11) becomes:

$$\dot{x} = \psi(x) + g(x)u + \bar{g}f, \quad (39)$$

where $f = [f_1, \dots, f_n]^T \in \mathcal{F} \subset \mathbb{R}^n$ is a total disturbance vector in each input channel, $\bar{g} = [\mathbf{0}_{n \times n}, \mathbf{I}_{n \times n}]^T$, $\mathbf{0}_{n \times n}$ and $\mathbf{I}_{n \times n}$ are $n \times n$ zero and identity matrices, respectively. Note that u and f are in the same channel, *i.e.*, the $n \times n$ matrix of the upper part of $g(x)$ is a zero matrix and each row in the lower part of $g(x)$ includes an independent input, so f is a matched disturbance vector.

To define safety sets for system (39), we consider an r -times continuously differentiable function $h(x)$, where the relative degrees of $h(x)$ with respect to both u and f are r , given that f is matched. A series of functions are defined as follows:

$$\begin{aligned} h_0(x) &= h(x), \\ h_1(x) &= \dot{h}_0(x) + \gamma_1 h_0(x), \\ &\vdots \\ h_r(x) &= \dot{h}_{r-1}(x) + \gamma_r h_{r-1}(x), \end{aligned} \quad (40)$$

where $\gamma_1, \dots, \gamma_r$ are positive constants. The corresponding series of safety sets are

$$\begin{aligned} \mathcal{C}_0 &= \{x \in \mathbb{R}^{2n} : h_0(x) \geq 0\}, \\ \mathcal{C}_1 &= \{x \in \mathbb{R}^{2n} : h_1(x) \geq 0\}, \\ &\vdots \\ \mathcal{C}_r &= \{x \in \mathbb{R}^{2n} : h_r(x) \geq 0\}. \end{aligned} \quad (41)$$

Theorem 2: For system (39), the relative degrees of $h(x)$ with respect to both the input u and the disturbance f are r , and f is known. If the initial states satisfy $x(0) \in \mathcal{C}_s = \bigcap_{j=0}^r \mathcal{C}_j$, then any Lipschitz continuous controller $u(x) \in K_{\text{cbf}}(t, x, f)$ renders the set \mathcal{C}_s forward invariant for system (39), where

$$K_{\text{cbf}}(t, x, f) \triangleq \{u \in \mathcal{U} : L_{\psi}^r h(x) + L_g L_{\psi}^{r-1} h(x)u + L_{\bar{g}} L_{\psi}^{r-1} h(x)f + \sum_{j=0}^{r-1} k_j h^{(j)}(x) \geq 0\}, \quad (42)$$

where $h^{(j)}(x)$ is the j th time derivative of $h(x)$, and $k_j, j = 0, \dots, r-1$, are the coefficients of polynomial $s^r + k_{r-1}s^{r-1} + \dots + k_0$ with roots at $-\gamma_1, \dots, -\gamma_r$.

Proof 2: From (40), h_r can be written as

$$h_r(x) = (s + \gamma_r)(s + \gamma_{r-1}) \cdots (s + \gamma_1)h(x) = s^r h(x) + k_{r-1}s^{r-1}h(x) + \cdots + k_0 h(x), \quad (43)$$

where $s \triangleq \frac{d}{dt}$. Since the control input u and disturbance f both have the same relative degree of r , u and f do not explicitly show in $h^{(j)}(x), 0 \leq j \leq r-1$ until

$$h^{(r)}(x) = L_{\psi}^r h(x) + L_g L_{\psi}^{r-1} h(x)u + L_{\bar{g}} L_{\psi}^{r-1} h(x)f. \quad (44)$$

By substituting (44) into (43) and comparing it with (42), the control values in $K_{\text{cbf}}(t, x, f)$ guarantee $h_r(x) \geq 0, \forall t > 0$. From the last equation in (40), we have $\dot{h}_{r-1}(x) + \gamma_r h_{r-1}(x) \geq 0$. Then $\dot{h}_{r-1}(x) \geq 0$ for any $x \in \partial \mathcal{C}_{r-1}$. According to Nagumo's theorem [32], since $x(0) \in \mathcal{C}_{r-1}$, we have $h_{r-1}(x) \geq 0, \forall t > 0$. Iteratively, $\dot{h}_0(x) + \gamma_1 h_0(x) \geq 0$, and we have $h_0(x) \geq 0, \forall t > 0$, as $x(0) \in \mathcal{C}_0$. Therefore, the set \mathcal{C}_s is forward invariant for system (39). This completes the proof of Theorem 2.

However, the disturbance vector f is not available in practice to enforce the inequality in (42). The estimated disturbance vector \hat{f} obtained in Subsection IV-B is used to devise our robust CBF. Then, (42) can be reformulated as:

$$K_{\text{cbf}}(t, x, f, \hat{f}) \triangleq \{u \in \mathcal{U} : L_{\psi}^r h(x) + L_g L_{\psi}^{r-1} h(x)u + L_{\bar{g}} L_{\psi}^{r-1} h(x)\hat{f} - L_{\bar{g}} L_{\psi}^{r-1} h(x)(\hat{f} - f) + \sum_{j=0}^{r-1} k_j h^{(j)}(x) \geq 0\}. \quad (45)$$

Since the disturbance estimation error $\hat{f} - f$ is unknown in (45), the following assumption is made for the disturbance estimation error bound of ESO.

The estimation error of \hat{f}_i is as follows [29]:

$$f_i(k) - \hat{f}_i(k) = p(k) * \Delta f_i(k), \quad (46)$$

where $*$ represents convolution and

$$p(k) = \begin{cases} 1 & 1 \leq k \leq r_i + 1 \\ \sum_{\iota=1}^{r_i+1} \frac{1}{(\iota-1)!} \left(\prod_{j=-\iota+1}^{-1} (k+j) \right) (1 - \omega_{o_i})^{\iota-1} \omega_{o_i}^{k-\iota} & k \geq r_i + 2. \end{cases} \quad (47)$$

For simplicity, let $\prod_{j=0}^{-1} (k+j) = 1$. Note that (46) is the disturbance estimation error formulated in the discrete-time domain. $f_i(k) = f_i(kT_s), \hat{f}_i(k) = \hat{f}_i(kT_s), \Delta f_i(k) = f_i((k+1)T_s) - f_i(kT_s), T_s$ is the sample time used in calculating

the error bound, and r_i and ω_{o_i} are the relative degree of \dot{q}_i (output measurement) with respect to f_i (disturbance as input) in the i -th joint subsystem and the poles of the i -th ESO in the discrete-time domain, respectively. Readers are referred to our previous work [29] for a complete proof of this error bound.

From the definition of derivative, Assumption 3, and (46), the disturbance estimation error bound of ESO is

$$|f_i(k) - \hat{f}_i(k)| \leq \Gamma_i(\omega_{o_i}, T_s) = \left(\sum_{k=1}^{\infty} p(k) \right) l_f T_s. \quad (48)$$

As mentioned in [25], although (48) is derived in the discrete-time domain, the disturbance estimation error bound obtained from it is still the same as that from the continuous-time domain. Since we need to utilize the disturbance estimation error bound in the continuous-time domain, T_s should be small, such as 0.1 ms, in our experiment setting. ω_{o_i} in the discrete-time domain needs to be converted from the continuous-time domain through Z-transform.

Theorem 3: Given the system (39) and the ESO in (22) under Assumption 3, any controller $u(x) \in K_{\text{rcbf}}$ renders the set \mathcal{C}_s forward invariant for system (39), where

$$K_{\text{rcbf}}(t, x, f, \hat{f}) \triangleq \{u \in \mathcal{U} : L_{\psi}^r h(x) + L_g L_{\psi}^{r-1} h(x)u + L_{\bar{g}} L_{\psi}^{r-1} h(x)\hat{f} - |L_{\bar{g}} L_{\psi}^{r-1} h(x)|\Gamma(\omega_o, T_s) + \sum_{j=0}^{r-1} k_j h^{(j)}(x) \geq 0\}, \quad (49)$$

$|L_{\bar{g}} L_{\psi}^{r-1} h(x)|$ denotes the absolute value of each element, and $\Gamma(\omega_o, T_s) = [\Gamma_1(\omega_{o_1}, T_s), \dots, \Gamma_n(\omega_{o_n}, T_s)]^T$.

Proof 3: From Theorem 2, we need to prove $h_r(x) \geq 0, \forall t > 0$. Substituting (44) and (48) into (43) yields

$$\begin{aligned} h_r(x) &= L_{\psi}^r h(x) + L_g L_{\psi}^{r-1} h(x)u + L_{\bar{g}} L_{\psi}^{r-1} h(x)f \\ &\quad + \sum_{j=0}^{r-1} k_j h^{(j)}(x) \\ &= L_{\psi}^r h(x) + L_g L_{\psi}^{r-1} h(x)u + L_{\bar{g}} L_{\psi}^{r-1} h(x)\hat{f} \\ &\quad - L_{\bar{g}} L_{\psi}^{r-1} h(x)(\hat{f} - f) + \sum_{j=0}^{r-1} k_j h^{(j)}(x) \\ &\geq L_{\psi}^r h(x) + L_g L_{\psi}^{r-1} h(x)u + L_{\bar{g}} L_{\psi}^{r-1} h(x)\hat{f} \\ &\quad - |L_{\bar{g}} L_{\psi}^{r-1} h(x)|\Gamma(\omega_o, T_s) + \sum_{j=0}^{r-1} k_j h^{(j)}(x) \geq 0. \end{aligned} \quad (50)$$

Then, we have $h_r(x) \geq 0, \forall t > 0$ as $x(0) \in \mathcal{C}_r$. Using the same procedure in Theorem 2, the set \mathcal{C}_s is forward invariant for system (39). This completes the proof of Theorem 3.

Remark 2: The key difference between our theoretical results in this work and our preliminary version [25] is that we have extended the robust CBF's safety guarantee from a relative degree of one to a general case of higher order CBF.

The safety specification requires the end-effector to maintain a non-negative distance from a virtual wall. The safety function is defined as $h(x) = y - y_0$, where y and y_0 denote the positions of the end-effector and the virtual wall, respectively. It can be verified that $h(x)$ has a relative degree of two [26]:

$$\begin{aligned} h_0 &= h, \\ h_1 &= \dot{h}_0 + \gamma h_0 = \dot{y} + \gamma(y - y_0), \\ h_2 &= \dot{h}_1 + \gamma h_1 = \ddot{y} + 2\gamma\dot{y} + \gamma^2(y - y_0), \end{aligned} \quad (51)$$

where a positive constant $\gamma_1 = \gamma_2 = \gamma$ is chosen,

$$\dot{y} = \left(\frac{\partial \zeta}{\partial q} \right) \dot{q}, \text{ and } \ddot{y} = \frac{d}{dt} \left(\frac{\partial \zeta}{\partial q} \right) \dot{q} + \frac{\partial \zeta}{\partial q} \ddot{q}.$$

Combining equations (11), (19), and (51) yields

$$h_2 = 2\gamma\dot{y} + \gamma^2(y - y_0) + \frac{d}{dt} \left(\frac{\partial \zeta}{\partial q} \right) \dot{q} + \frac{\partial \zeta}{\partial q} \left(-\bar{M}^{-1}(\bar{C}\dot{q} + \bar{G} - \bar{K}_d\dot{q}_d) + f \right). \quad (52)$$

To simultaneously achieve tracking and safe control, the nominal controller for \dot{q}_d , designed in (24), should be minimally intervened. Thus, the following QP-CBF is constructed:

$$\begin{aligned} \dot{q}_{d\text{safe}} &= \arg \min_{u \in \mathcal{U}} \|u - \dot{q}_d\|^2 \\ \text{s.t. } & h_i(x(0)) > 0, \quad i = 0, 1, 2 \\ & L_\psi^2 h(x) + L_g L_\psi h(x) u \\ & + L_{\bar{g}} L_\psi h(x) \hat{f} - |L_{\bar{g}} L_\psi h(x)| \Gamma(\omega_o, T_s) \\ & + 2\gamma\dot{h}(x) + \gamma^2 h(x) \geq 0. \end{aligned} \quad (53)$$

V. HARDWARE EXPERIMENTS

We use the PUMA 500 robot for hardware experiments, as shown in Fig. 3. It has three main joints and a spherical wrist, providing six degrees of freedom. q_1 , q_2 , and q_3 correspond to the waist, shoulder, and elbow joints, while q_4 , q_5 , and q_6 represent the wrist rotation, bend, and flange angles. Since our focus is task-space tracking (*i.e.*, wrist center position), only the first three joints are used. Each joint is driven by a DC motor powered by an Adept Technology MV-19 Power Chassis. The control program is built in MATLAB Simulink, which generates C code and an SDF file, and runs via a dSPACE 1103 for control and data acquisition.

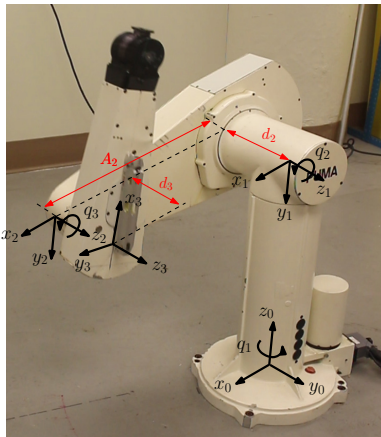


Fig. 3. PUMA 500 robot used as a testbed in our research.

The inner-loop controller is configured as $\tau = -K_p(q - q_d) - K_d(\dot{q} - \dot{q}_d)$, where $K_p = \text{diag}([18, 144, 9])$ and $K_d = \text{diag}([18, 12, 9])$. The gains are non-round values due to the actuator driver's voltage-to-torque conversion ratio. The structure and true parameters remain unknown to our outer-loop controller. The nominal second-order system model (12) is used for the controller. The reference trajectory for joints q_1 , q_2 , and q_3 is $[0.5 \sin(t) \quad 0.25 \sin(2t) + 0.534 \quad 0.25 \sin(2t) + \frac{\pi}{2}]^T$.

The tracking performance of the nominal inner-loop controller is illustrated in Fig. 4. Specifically, Fig. 4a depicts the trajectory tracking performance in the joint space, while Fig. 4b shows the trajectory tracking performance in the Cartesian space. The results indicate that the inner-loop controller exhibits poor tracking performance. We will demonstrate the improvement achieved by adding our approach to the tracking and safe control tasks.

We use the nominal model (12) throughout the experiments. A key parameter in the controller design is the control gain in (24), $b_0 \triangleq \bar{M}^{-1} \bar{K}_d$, which depends on the nominal inertia matrix \bar{M} and the inner-loop proportional gain. The nominal inertia \bar{M} is adopted from [33]. Following a common ESO tuning rule, we tune each joint individually by initially setting b_0 large to ensure stability and then gradually reducing it to improve tracking accuracy. The final nominal control gain is $\text{diag}([20, 40, 10])$. The observer and control bandwidths are set to 80 rad/s and 10 rad/s, respectively, for each joint. We refer readers to [34] for additional instructions and theoretical support on tuning nominal control gain.

A. Tracking Control

We compare the tracking performance of ours, with [2]. The reason is that we share the same minimal assumptions about the inner-loop controller, which, to the best of our knowledge, are the most general in the literature.

1) **Scenario 1: Normal Case without Payload:** The robot tracks a reference trajectory without a payload. The tracking performance of the learning-based adaptive controller [2] and ours is shown in Fig. 5. Fig. 5a compares the reference (dashed) and actual joint trajectories of q_1 , q_2 , and q_3 , where blue and red lines represent our method and [2], respectively. The x-axis denotes time (s), and the y-axis denotes joint angles (rad). Fig. 5b shows the Cartesian trajectories in x , y , and z . The close alignment of the final and reference trajectories indicates that both controllers achieve accurate tracking despite model uncertainties and an imperfect inner loop.

The proposed method achieves tracking performance comparable to the learning-based adaptive controller in the no-payload experiment. As shown in Fig. 6, both approaches yield similarly smooth control signals. Transient responses occur initially, particularly in the second joint (Fig. 5a), due to the offset between the initial and reference positions. The learning-based controller exhibits a longer transient phase (see Figs. 5a and 6). This reflects a typical trade-off in adaptive control between transient duration and tracking accuracy.

2) **Scenario 2: Robustness Testing with Different Payloads:** We evaluate controller robustness with payloads of 1 kg, 1.5 kg, and 2 kg attached to the end-effector. Each payload experiment is repeated five times for ANOVA analysis, with identical controller and observer parameters. Fig. 7a and Fig. 7b present the tracking error ANOVA results for both methods. As shown earlier, our approach achieves a shorter transient time than the learning-based adaptive controller. For clarity, transient data (first 5 s) are excluded, and the plots show steady-state tracking errors (after 5 s).

As shown in Fig. 7a, the ANOVA results indicate that our method maintains statistically consistent errors across different

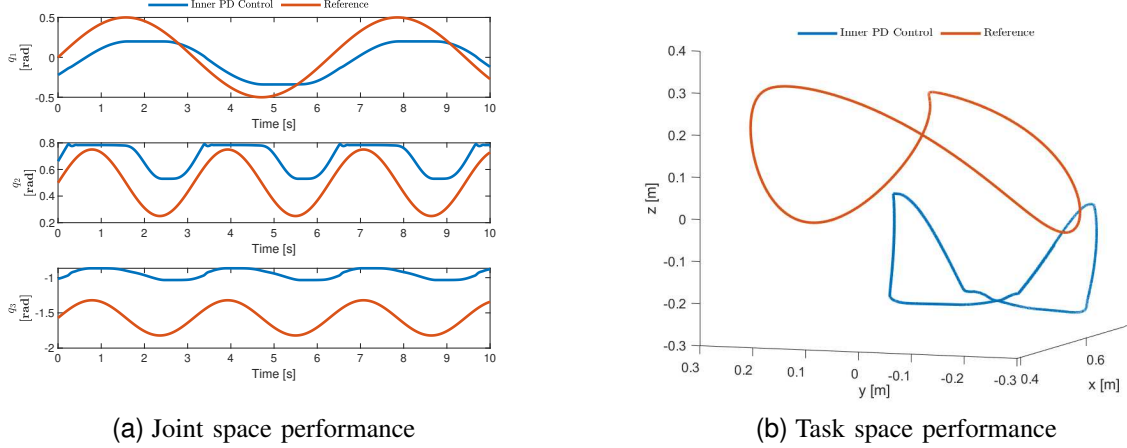


Fig. 4. Poor inner-loop PD controller's performance for 10 s. (a) Trajectory tracking performance in the joint space. (b) Trajectory tracking performance in the Cartesian space. The inner-loop controller can not track the reference trajectory.

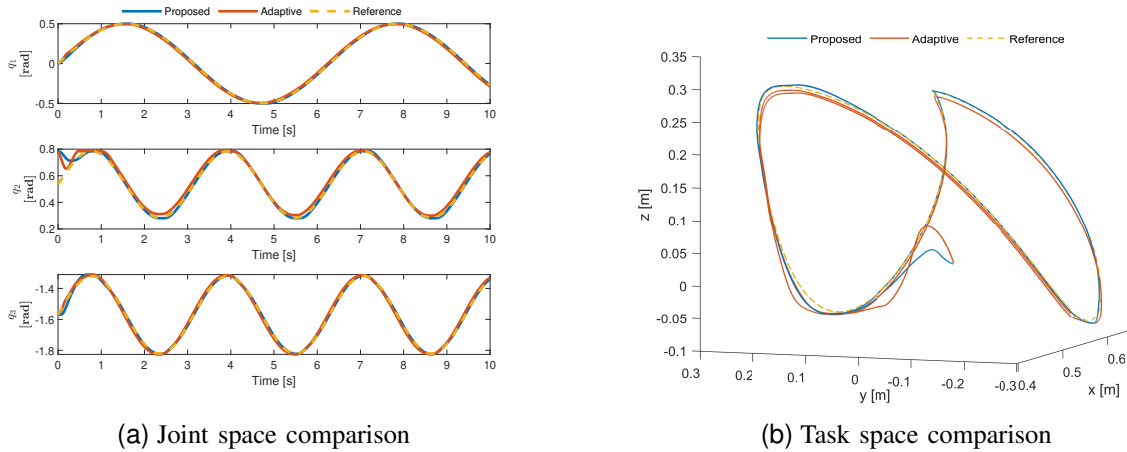


Fig. 5. Comparative tracking precision analysis: (a) Root Mean squared error (RMSE) in joint space: Proposed (4.1×10^{-3} , 2.76×10^{-2} , 7.6×10^{-3}) radians vs. [2] (4.3×10^{-3} , 2.7×10^{-2} , 5.7×10^{-3}) radians for each joint. (b) Cartesian tracking error RMSE: Proposed (2.3 mm, 2.4 mm, 15.5 mm) vs. [2] (2.9 mm, 2.1 mm, 16.1 mm) for each joint. Data sampled at 1 kHz over a 10 s trajectory execution.

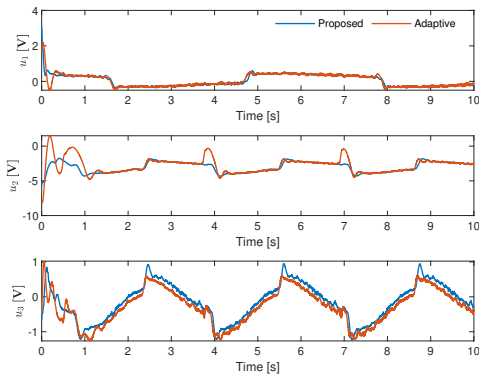


Fig. 6. Inner-loop control command comparison for 10 s. u_1 , u_2 , and u_3 are the control inputs (voltages) for joint q_1 , q_2 , and q_3 , respectively.

payloads ($p > 0.05$), demonstrating strong robustness, whereas the adaptive method shows significant variations with payload

changes ($p < 0.05$).

In summary, our approach offers several advantages over the learning-based adaptive control [2]. As shown in Fig. 5, it achieves comparable tracking performance without a payload, lower steady-state error, and stable performance under varying payloads (Fig. 7). It also exhibits a shorter transient response, as seen in the trajectories and control signals during the first second (Figs. 5 and 6). Moreover, our design is simpler than a neural network, requiring fewer tunable parameters and offering greater interpretability. Finally, the proposed disturbance compensation supports both tracking and safe control with state constraints, whereas [2] cannot handle constraints.

B. Safe Control

It is worth noting that γ in (53) critically influences the CBF's behavior. A larger γ drives the trajectory closer to the safety set boundary (more aggressive), while a smaller γ keeps it farther away (more conservative). To achieve a safe yet efficient controller, we set $\gamma = 10$ in all experiments.

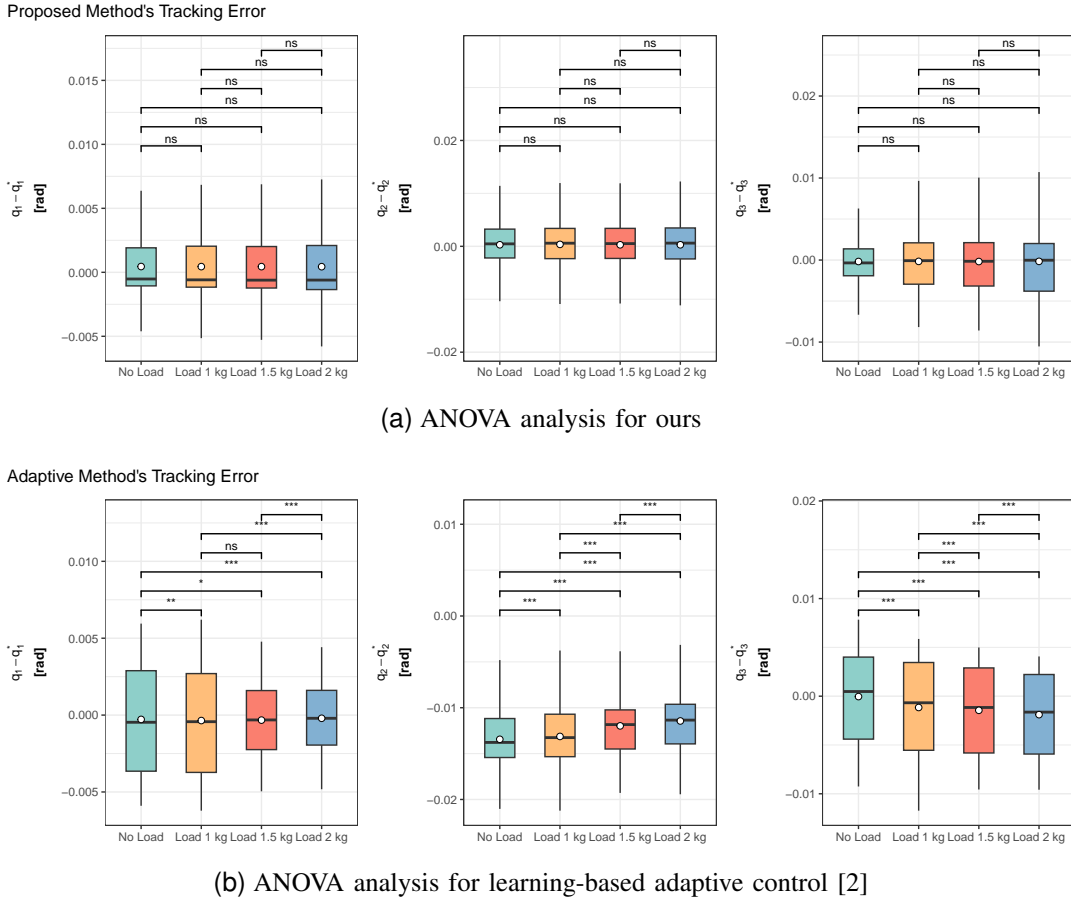


Fig. 7. Steady-state tracking error comparison under different payloads. (a) ANOVA of ours. (b) ANOVA of the learning-based adaptive control [2]. The proposed method shows consistent tracking across payloads, as indicated by uniform box plots, while the adaptive method exhibits larger error variations, implying reduced robustness. Significance levels: ns ($p > 0.05$), * ($p \leq 0.05$), ** ($p \leq 0.01$), *** ($p \leq 0.001$). Each experiment is repeated five times.

We have conducted experiments in three scenarios: (1) Safety and Robustness Testing with Different Payloads, (2) Safety Testing Subject to External Disturbance, and (3) Safety Testing Subject to Gravity Disturbance. The first scenario will be described in detail, whereas the second and third scenarios are demonstrated in our accompanying video.

A virtual boundary is defined at $y_0 = [y_1 \ -0.1 \ y_3]^T$ as a spatial constraint for the end effector. It moves freely along the x and z axes but is constrained along the y axis with a lower limit of -0.1 m. The system is tested with payloads of 1, 1.5, and 2 kg attached to the end effector.

Three approaches are compared: (1) conventional CBF with a nominal model (see Fig. 8); (2) our robust CBF with a nominal model and an ESO for disturbance estimation, compared to the DOB-CBF [16] (see Fig. 9a); and (3) our robust CBF with a nominal model, ESO for disturbance estimation, and estimation error bound, compared to the DOB-CBF with estimation error bound (see Fig. 9b).

Fig. 8 shows the safety performance of the CBF using only the nominal second-order model (12), which neglects model errors, inner-loop uncertainty, and external disturbances. The safety function h varies under different payloads, revealing limited robustness.

We implement the DOB-CBF [16] for comparison. The DOB-CBF estimates $b_e(x, d) = \frac{\partial \zeta}{\partial q} f$ in the CBF, while our

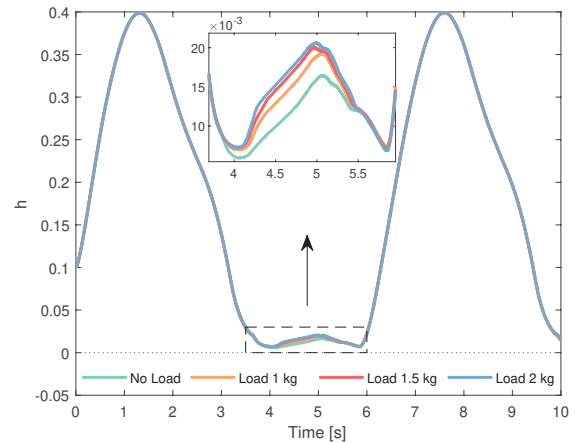


Fig. 8. **Safety boundary:** $y_0 = [y_1 \ -0.1 \ y_3]^T$. Conventional CBF with nominal model: safety performance with variances under different payloads, with the lowest value of h function at 5.9 mm.

method directly estimates f in the original dynamics. Thus, the two observers target different quantities, and their gains are not directly comparable. For fairness, excluding error bounds, we tune both observers' gains to achieve similar minimum h magnitudes, indicating comparable safety performance. Fig. 9a compares the h functions of the DOB-CBF and the proposed

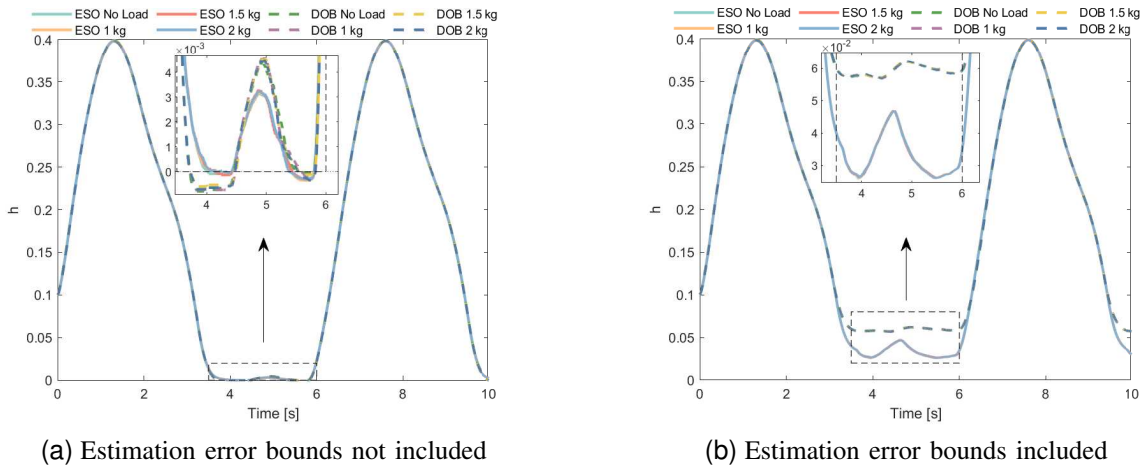


Fig. 9. Safety boundary: $y_0 = [y_1 \ -0.1 \ y_3]^T$. (a) CBFs with the nominal model and disturbance compensation by ESO (solid lines) and DOB (dashed lines) show consistent (robust) safety performance under different payloads, with the lowest h value being -0.366 mm (unsafe) for our method and -0.597 mm (unsafe) for the DOB-CBF. (b) CBFs with the nominal model, disturbance compensation by ESO (solid lines) and DOB (dashed lines), and error bounds show consistent (robust) safety performance under different payloads, with the lowest h value being 26.1 mm (safe and less conservative) for our method and 56.8 mm (safe and more conservative) for the DOB-CBF.

method, showing that:

- 1) The safety function h exhibits consistent performance under different payloads, indicating robustness of both methods.
- 2) A slight safety violation occurs due to disturbance estimation error, with minimum values of -0.597 mm for DOB-CBF and -0.366 mm for the proposed method, highlighting the need to account for estimation error bounds in both.

We collect experimental data for $\hat{b}_e(x, d)$ and \hat{f} from the DOB and ESO, respectively. Their finite differences yield the maximum rates of change, used as estimation error bounds. Fig. 9b shows the resulting h values after incorporating these bounds. Compared with Fig. 9a, we observe that:

- 1) The trajectories remain safe and consistent across different payloads, demonstrating the robustness of both methods.
- 2) Incorporating the estimation error bound raises h , keeping trajectories strictly within the safety set (positive h values).
- 3) With error bounds, our method stays closer to the safety boundary than [16], indicating lower conservatism. This may be because [16] estimates $b_e(x, d) = \frac{\partial \zeta}{\partial q} f$, which includes a state-dependent Jacobian, making it more sensitive to measurement noise and compounding estimation errors.

VI. CONCLUSION AND FUTURE WORK

This paper presents a unified framework that improves tracking performance and ensures safe kinematic control for closed-architecture robotic systems. The proposed method integrates seamlessly into existing cascade control structures as an add-on, enabling robust and safe control under uncertain dynamics, external disturbances, and unknown inner-loop controllers. Stability and safety are theoretically guaranteed, and real-time validation is conducted on the PUMA 500

industrial robot. Future work will extend the framework to visual servoing systems, addressing uncertainties in the vision pipeline.

REFERENCES

- [1] H. Wang, W. Ren, C. C. Cheah, Y. Xie, and S. Lyu, "Dynamic modularity approach to adaptive control of robotic systems with closed architecture," *IEEE Transactions on Automatic Control*, vol. 65, no. 6, pp. 2760–2767, 2019.
- [2] J. J.-B. M. Ahanda, A. Melingui, O. Lakhali, B. E. Zobo, H. Kadri, and R. Merzouki, "Adaptive tracking control for industrial robot manipulators with unknown inner loop architecture," in *2022 International Conference on Robotics and Automation*. IEEE, 2022, pp. 9860–9866.
- [3] J. J.-B. M. Ahanda, C. M. Aba, A. Melingui, B. E. Zobo, and R. Merzouki, "Task-space control for industrial robot manipulators with unknown inner loop control architecture," *Journal of the Franklin Institute*, vol. 359, no. 12, pp. 6286–6310, 2022.
- [4] G. D. Khan, "Control of robot manipulators with uncertain closed architecture using neural networks," *Intelligent Service Robotics*, pp. 1–13, 2024.
- [5] W. Liu, S. Zhang, J. Lin, Y. Xia, J. Wang, and Y. Sun, "Advancements in accuracy decline mechanisms and accuracy retention approaches of CNC machine tools: a review," *The International Journal of Advanced Manufacturing Technology*, vol. 121, no. 11, pp. 7087–7115, 2022.
- [6] T. G. Molnar, R. K. Cosner, A. W. Singletary, W. Ubellacker, and A. D. Ames, "Model-free safety-critical control for robotic systems," *IEEE Robotics and Automation Letters*, vol. 7, no. 2, pp. 944–951, 2021.
- [7] A. Singletary, S. Kolathaya, and A. D. Ames, "Safety-critical kinematic control of robotic systems," *IEEE Control Systems Letters*, vol. 6, pp. 139–144, 2021.
- [8] T. G. Molnar and A. D. Ames, "Safety-critical control with bounded inputs via reduced order models," in *2023 American Control Conference*. IEEE, 2023, pp. 1414–1421.
- [9] M. Jankovic, "Robust control barrier functions for constrained stabilization of nonlinear systems," *Automatica*, vol. 96, pp. 359–367, 2018.
- [10] S. Kolathaya and A. D. Ames, "Input-to-state safety with control barrier functions," *IEEE Control Systems Letters*, vol. 3, no. 1, pp. 108–113, 2019.
- [11] A. Alan, A. J. Taylor, C. R. He, G. Orosz, and A. D. Ames, "Safe controller synthesis with tunable input-to-state safe control barrier functions," *IEEE Control Systems Letters*, vol. 6, pp. 908–913, 2021.
- [12] J. Buch, S.-C. Liao, and P. Seiler, "Robust control barrier functions with sector-bounded uncertainties," *IEEE Control Systems Letters*, vol. 6, pp. 1994–1999, 2022.
- [13] Q. Nguyen and K. Sreenath, "Robust safety-critical control for dynamic robotics," *IEEE Transactions on Automatic Control*, vol. 67, no. 3, pp. 1073–1088, 2022.

- [14] A. Alan, T. G. Molnar, A. D. Ames, and G. Orosz, "Parameterized barrier functions to guarantee safety under uncertainty," *IEEE Control Systems Letters*, vol. 7, pp. 2077–2082, 2023.
- [15] Y. Wang and X. Xu, "Disturbance observer-based robust control barrier functions," in *2023 American Control Conference*, 2023, pp. 3681–3687.
- [16] E. Daş and R. M. Murray, "Robust safe control synthesis with disturbance observer-based control barrier functions," in *2022 IEEE 61st Conference on Decision and Control*. IEEE, 2022, pp. 5566–5573.
- [17] A. Alan, T. G. Molnar, E. Daş, A. D. Ames, and G. Orosz, "Disturbance observers for robust safety-critical control with control barrier functions," *IEEE Control Systems Letters*, vol. 7, pp. 1123–1128, 2023.
- [18] P. Zhao, Y. Mao, C. Tao, N. Hovakimyan, and X. Wang, "Adaptive robust quadratic programs using control Lyapunov and barrier functions," in *2020 59th IEEE Conference on Decision and Control*. IEEE, 2020, pp. 3353–3358.
- [19] J. Sun, J. Yang, and Z. Zeng, "Safety-critical control with control barrier function based on disturbance observer," *IEEE Transactions on Automatic Control*, vol. 69, no. 7, pp. 4750–4756, 2024.
- [20] E. Daş and J. W. Burdick, "Robust control barrier functions using uncertainty estimation with application to mobile robots," *IEEE Transactions on Automatic Control (Early Access)*, 2025.
- [21] X. Wang, J. Yang, C. Liu, Y. Yan, and S. Li, "Safety-critical disturbance rejection control of nonlinear systems with unmatched disturbances," *IEEE Transactions on Automatic Control (Early Access)*, 2025.
- [22] Z. Cao, J. Mao, C. Zhang, C. Cui, and J. Yang, "Safety-critical generalized predictive control for speed regulation of PMSM drives based on dynamic robust control barrier function," *IEEE Transactions on Industrial Electronics*, vol. 72, no. 2, pp. 1881–1891, 2025.
- [23] S. Zhang, D.-H. Zhai, J. Lin, Y. Xiong, Y. Xia, and M. Wei, "ESO-based safety-critical control for robotic systems with unmeasured velocity and input delay," *IEEE Transactions on Industrial Electronics*, vol. 71, no. 10, pp. 13 053–13 063, 2024.
- [24] H. Wang, J. Peng, F. Zhang, and Y. Wang, "A composite control framework of safety satisfaction and uncertainties compensation for constrained time-varying nonlinear MIMO systems," *IEEE Transactions on Systems, Man, and Cybernetics: Systems*, vol. 53, no. 12, pp. 7864–7875, 2023.
- [25] J. Chen, Z. Gao, and Q. Lin, "Robust control barrier functions for safe control under uncertainty using extended state observer and output measurement," in *2023 62nd IEEE Conference on Decision and Control*. IEEE, 2023, pp. 8477–8482.
- [26] Q. Nguyen and K. Sreenath, "Exponential control barrier functions for enforcing high relative-degree safety-critical constraints," in *2016 American Control Conference*. IEEE, 2016, pp. 322–328.
- [27] W. Xiao and C. Belta, "Control barrier functions for systems with high relative degree," in *2019 IEEE 58th Conference on Decision and Control*. IEEE, 2019, pp. 474–479.
- [28] A. D. Ames, X. Xu, J. W. Grizzle, and P. Tabuada, "Control barrier function based quadratic programs for safety critical systems," *IEEE Transactions on Automatic Control*, vol. 62, no. 8, pp. 3861–3876, 2017.
- [29] J. Chen, Z. Gao, Y. Hu, and S. Shao, "A general model-based extended state observer with built-in zero dynamics," *arXiv preprint arXiv:2208.12314*, 2023.
- [30] Z. Gao, "Scaling and bandwidth-parameterization based controller tuning," in *2003 American Control Conference*. IEEE, 2003, pp. 4989–4996.
- [31] L. Perko, *Differential equations and dynamical systems*. Springer Science & Business Media, 2013, vol. 7.
- [32] F. Blanchini, S. Miani *et al.*, *Set-theoretic methods in control*. Springer, 2008, vol. 78.
- [33] P. Khalaf and H. Richter, "Trajectory optimization of robots with regenerative drive systems: Numerical and experimental results," *IEEE Transactions on Robotics*, vol. 36, no. 2, pp. 501–516, 2019.
- [34] W. Xue and Y. Huang, "Performance analysis of active disturbance rejection tracking control for a class of uncertain LTI systems," *ISA Transactions*, vol. 58, pp. 133–154, 2015.



Fan Zhang received the B.S. degree in Telecommunications from Nanjing University of Posts and Telecommunications, Nanjing, China, in 2016, and the M.S. degree in Electrical Engineering from Iowa State University, Ames, IA, USA, in 2019. He is currently pursuing the Ph.D. degree in Electrical Engineering at the University of Houston, Houston, TX, USA. His current research focuses on safe control of robotics under disturbances.



Jinfeng Chen is a Postdoctoral Fellow in the Department of Engineering Technology at the University of Houston, Houston, TX, USA. His research interests include active disturbance rejection control, unknown input observer design, safety control, and multi-target tracking.



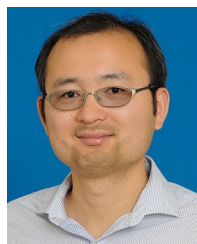
Joseph Jean-Baptiste Mvogo Ahanda received the Ph.D. degree in robotics from the University of Yaoundé 1, Yaoundé, Cameroon, in 2019. He is currently with the Department of Biomedical Engineering, The University of Ebolowa, Cameroon. His research interests include system modeling, intelligent control, adaptive control, robust control, and robotics.



Hanz Richter received the B.Sc. degree from Pontificia Universidad Católica del Perú, Lima, Peru, in 1995, the M.Sc. and Ph.D. degrees from the Oklahoma State University, Stillwater, OK, USA, in 1997 and 2001, respectively, all in mechanical engineering. He is currently a Professor of Mechanical Engineering with Cleveland State University, Cleveland, OH, USA. His current research interests include the broad areas of control, robotics, and mechatronics with applications to biomedical robotics, aerospace propulsion, high-precision motion control and smart sensors. His research funding has been supported by the U.S. National Science Foundation, NASA, the State of Ohio, the Parker–Hannifin Corporation and the Cleveland Clinic Foundation.



Ge Lv received the B.S. degree in automation and the M.S. degree in control theory and control engineering from Northeastern University, Shenyang, China, in 2011 and 2013, respectively, and the Ph.D. degree in electrical engineering from The University of Texas at Dallas, in 2018. He is currently an Assistant Professor with the Department of Mechanical Engineering and Department of Bioengineering, Clemson University. Prior to joining Clemson University, in Spring 2020, he was a Postdoctoral Fellow with the Robotics Institute, Carnegie Mellon University. His research interests include the control and human-in-the-loop optimization of lower-limb wearable robots. He received the Best Student Paper Award from the 2015 IEEE Conference on Decision and Control and the Faculty Early Career Development Program (CAREER) Award from the National Science Foundation, in 2024.



Bin Hu received the M.S. degree in control and system engineering from Zhejiang University, Hangzhou, China, in 2010, and the Ph.D. degree from The University of Notre Dame, Notre Dame, IN, USA, in 2016. He is currently Assistant Professor with the Department of Engineering Technology, University of Houston, Houston, TX, USA. His research interests include machine learning in networked control systems, cybersecurity, distributed control and optimization, and human robot interaction.



Qin Lin received the Ph.D. degree in Computer Science from Delft University of Technology (TU Delft), Delft, The Netherlands, in 2019.

He is an Assistant Professor jointly appointed by the Department of Engineering Technology and the Department of Electrical and Computer Engineering at the University of Houston, Houston, TX, USA. From 2019 to 2021, he was a Postdoctoral Fellow at the Robotics Institute, Carnegie Mellon University, Pittsburgh, PA, USA. His research interests span robotics, machine learning, control, and formal verification. He also serves as an Associate Editor for the IEEE/RSJ INTERNATIONAL CONFERENCE ON INTELLIGENT ROBOTS AND SYSTEMS, IEEE TRANSACTIONS ON VEHICULAR TECHNOLOGY, and IEEE ROBOTICS AND AUTOMATION LETTERS.